Improved Crystalline Quality and Self-Field J_c in Sequentially Vacuum-Multilayered YBCO Thin Films on Buffered Metallic Templates

M. M. Aye ⓘ, E. Rivasto, T. Vaimala, Y. Zhao ⓘ, *Senior Member, IEEE*, H. Huhtinen ⓘ, and P. Paturi ⓘ

Abstract—The effect of simple *in situ* vacuum treatment between the sequentially multilayered YBCO thin films by pulsed laser deposition is investigated. The vacuum treatment during the growth intervals is observed to have a diminishing effect on the formation of structural defects along the *c*-axis of the YBCO lattice. This greatly improves the structural properties of the film, ultimately resulting in almost 40% increased self-field critical current density. The underlying mechanisms behind the vacuum treatment are comprehensively discussed with the help of Kinetic Monte Carlo simulations, suggesting that the improved crystalline quality of each sublayer results from desorption of weakly bound atomic species from the film surface thus reducing probability of defect formation in the following ablation interval.

Index Terms—HTS, YBCO, multilayers, thin film growth, crystalline quality, flux pinning, critical current density.

I. INTRODUCTION

TO MAXIMIZE the absolute critical current density J_c of YBCO thin films and coated conductors at high magnetic fields favourable for electric power applications [1], [2], [3], [4], [5], [6], [7], requirements of both the high crystalline quality and optimal flux pinning properties should be fulfilled [8], [9], [10]. The flux pinning structure organized with an artificially produced nanocolumn network within the YBCO matrix that maximally pins the vortices is widely studied [11], [12], [13], [14], [15], [16], [17], but the formation of crystalline defects that directly affect the shortening of the electron mean free path and thus the zero-field critical current density has got less attention in the field of high-temperature superconductors [9], [18], [19], [20], [21]. In the zero- and low-field applications below ≈100 mT, the crystalline structure of YBCO is solely

responsible for maximum J_c and in the mid-field applications between 100 mT and ≈2 T, the J_c at the zero-field unambiguously limits the in-field properties [10].

Solving the difficulties of depositing thick YBCO films of high crystalline quality has been tried by many different methods, where at least off-axis deposition [22], [23], [24], [25], [26], various buffer layer structures [27], [28], [29], [30], [31], complicated high-rate or rapid interval depositions [32], [33], [34] have brought the desired improvement in YBCO microstructure, by affecting the growth mechanism and decreasing the formation of the defects through the YBCO lattice. Since the crystalline growth is greatly dependent on the relaxation of the substrate induced strain and the formation of the dislocations, the optimal thickness with epitaxial growth defines the limit above which self-field $J_c(0)$ starts to decrease dramatically. Therefore, by limiting the thickness of the single layer, but forming a multilayer structure from the several individual layers that are separated by a very thin layer of other oxige such as CeO_2 or $SrTiO_3$ [35], [36], [37], [38] has also been successfully used for improving the self-field properties. Since these methods consisting of multilayers of several oxides are usually complicated to realize as well as they are time and material consuming, we have tried to focus on the simple *in situ* deposition method producing sequentially multilayered undoped YBCO thin films, where during the intervals the relaxation of the interface layer in vacuum has been carried out. Based on the structural and magnetic chaeracterizations of the films, we have obtained clearly improved properties in YBCO thin films deposited on buffered metallic templates.

II. EXPERIMENTAL DETAILS

The YBCO multilayers of various layer thicknesses were manufactured by pulsed laser deposition (PLD) from the nanocrystalline YBCO target [7], [39] on metallic template (Hastelloy C276) with an advanced $Al_2O_3/Y_2O_3/IBAD\text{-}MgO/LaMnO_3/CeO_2$ buffer layer structure (Fig. 1). The multilayer structures of 4×500 (4 L:VAC) and 8×250 (8 L:VAC) pulses producing 4×95 nm and 8×47 nm layer thicknesses were deposited applying 2 min vacuum treatment of 10^{-3} torr between the layers. The details of the PLD system and buffer layer structures are given elsewhere [7], [40]. The crystalline quality was studied by x-ray diffractometry (XRD) with PANalytical Empyrean diffractometer in Bragg-Brentano mode. The incident
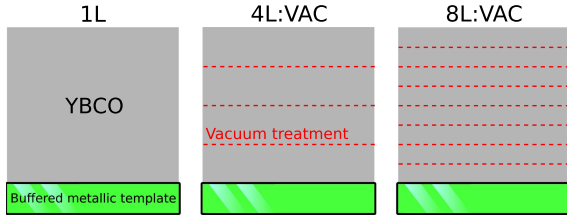
Fig. 1. The schematic diagram of the multilayer structures, where 4×500 (4 L:VAC) and 8×250 (8 L:VAC) pulses of YBCO were deposited with 2 min vacuum treatment between the layers. The film structures were deposited on the metallic hastelloy C276 template with IBAD-MgO based buffer layers and the YBCO single layer film of 2000 pulses (1 L) is prepared for comparison. The total thickness of 1 L, 4 L:VAC and 8 L:VAC films is ≈ 380 nm.

TABLE I
STRUCTURAL PROPERTIES OF YBCO FILMS DETERMINED BY XRD
MEASUREMENTS.

Sample	$c(\text{Å})$	$\Delta\theta(°)$	$\Delta\phi(°)$	$\Delta\omega(°)$	$I(005)/I(004)$
1L	11.73	0.27	3.40	2.49	13.1
4L:VAC	11.72	0.22	3.39	2.24	12.7
8L:VAC	11.73	0.21	2.85	2.12	13.7

x-ray beam was collimated with a Bragg-Brentano$^{\text{HD}}$ mirror, using a 1/4° divergence slit and 0.04 rd Soller. A PIXcel$^{\text{3D}}$ was used as a detector. High-resolution transmission electron microscopy (HRTEM) was performed with a JEOL JEM-2200FS electron microscope combined with 200 kV field emission gun (FEG) and in-column energy filter (Omega filter). In addition, a probe-corrected scanning TEM using high-angle annular dark-field imaging (HAADF STEM) was performed with Titan 80-300 at the voltage of 200 kV. The magnetic properties of the films were investigated with a Quantum Design PPMS system, where the critical temperatures were determined from the ac magnetization curves and the magnetic field dependences of the critical current densities from the opening of the hysteresis loops using the Bean model for rectangular films. The angular dependent transport properties with angular range from 0 to 360° were measured using a horizontal rotation option of the PPMS. The accommodation field B^*, which is defined as an upper limit of the low-field plateau of $J_c(B)$, was determined by the criterion $J_c(B)/J_c(0) = 0.9$ [41].

III. RESULTS AND DISCUSSION

A. Vacuum Treatment Governed Structural Properties

The effect of multilayering in crystalline quality and formation of structural defects were studied by XRD and the collection of the most important parameters is shown in Table I. As can be seen, the length of the c-axis of the YBCO unit cell as well as the intensity ratio between the peaks $I(005)/I(004)$ do not systematically vary in single layer and multilayered films, indicating similar oxidation level in all the films. Instead, as can be seen in Fig. 2, the broadening of the XRD peaks is clearly diminished in all θ, ϕ and ω directions. This unambiguously demonstrates that the variation in the unit cells and the number of structural defects such as low-angle grain boundaries are reduced
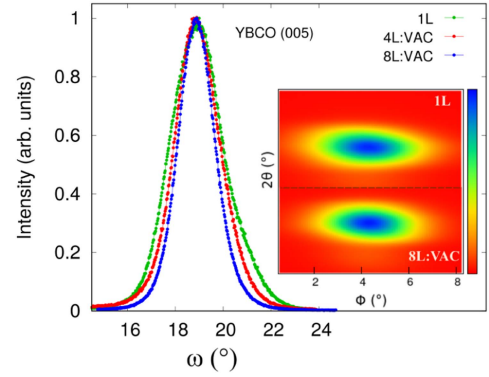

Fig. 2. The normalized XRD rocking curves (ω-scans) of the YBCO (005) peaks measured from the YBCO multilayers (the main panel). In the inset, the XRD (102) peaks as functions of 2θ and relative ϕ are given for the samples 1 L and 8 L:VAC.
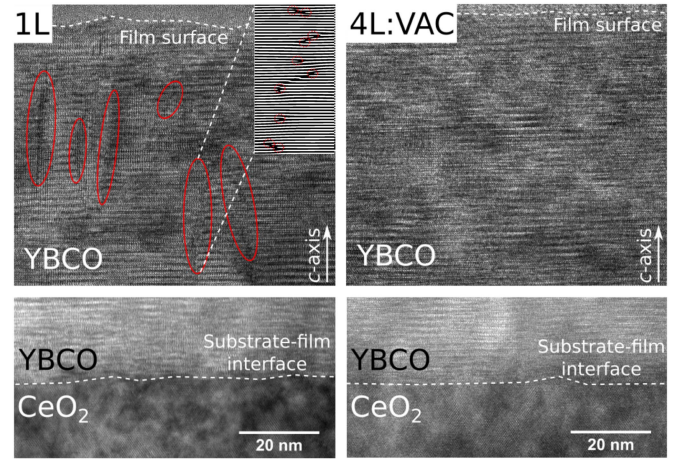

Fig. 3. Cross-sectional HRTEM images of samples 1 L and 4 L:VAC, where the upward direction corresponds to YBCO c-axis. The bottom images in both 1 L and 4 L:VAC are taken from the interface of top buffer layer CeO$_2$, while the images on the top are from the surface layer of the films. The red markings on the image of film 1 L indicate the edge dislocations collectively positioned along the YBCO c-axis, as also shown in the inverse FFT image on the top right corner.

by multilayering and the unit cells are much better aligned, increasing the out-of-plane lattice ordering in multilayered YBCO films [42].

Based on the cross-sectional HRTEM images of samples 1 L and 4 L:VAC shown in Fig. 3, we can conclude that there are similar types of edge dislocations along the a/b-plane from the substrate interface through the whole film in both 1 L and 4 L:VAC films. However, as can be seen in the images taken from the surface, the greater number of edge dislocations in 1 L film are mainly oriented in chains along the YBCO c-axis, being nicely in accordance with our XRD results. This clearly shows that our vacuum-multilayering remarkably reduces the formation of structural defects in the YBCO matrix.

B. Improvements in Superconducting Properties

As shown in Fig. 4(a), $T_{c,\text{onset}}$s are almost the same in all 1 L, 4 L:VAC and 8 L:VAC films. However, the transition is clearly
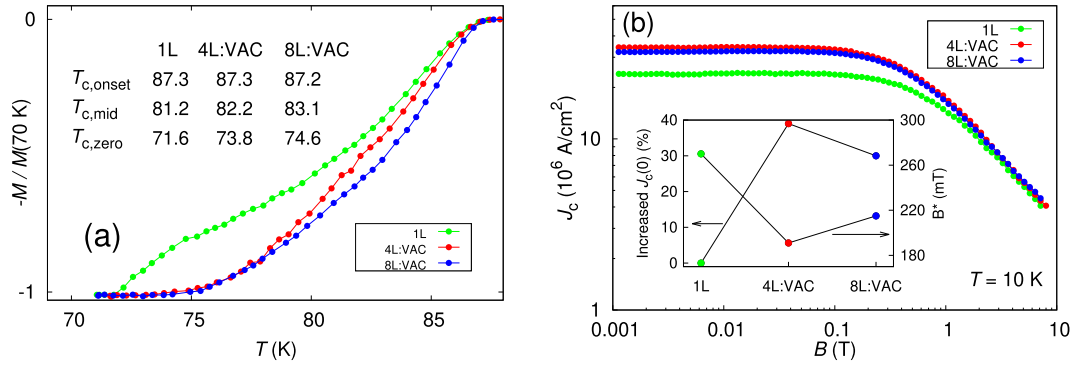
Fig. 4.   (a) The normalized ac magnetizations as functions of temperature. The inset table shows differently determined critical temperatures from the onset temperature $T_{c,\mathrm{onset}}$, zero level $T_{c,\mathrm{zero}}$ and from the middle of the transition $T_{c,\mathrm{mid}}$. (b) The magnetic field dependences of J_c determined from the magnetic hysteresis loops at 10 K. The inset shows how the multilayering in vacuum increases the $J_c(0)$ but decreases B^* in films 1 L, 4 L:VAC and 8 L:VAC.
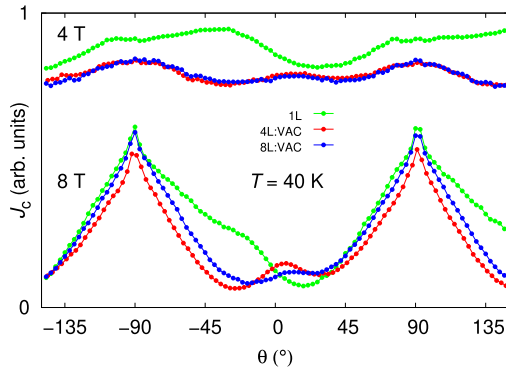

Fig. 5.   The angular dependences of J_c measured in 4 T and 8 T fields at 40 K for single layer 1 L and multilayered 4 L:VAC and 8 L:VAC films.

narrower when increasing the number of vacuum treatments during the deposition and thus the second phase starting around 80 K in 1 L film disappear in both multilayered films, being in line with their higher $T_{c,\mathrm{mid}}$ and $T_{c,\mathrm{zero}}$ values. When looking at the $J_c(B)$ curves in Fig. 4(b), we can obtain that multilayering significantly increases J_c below the magnetic field of 1 T. As shown in the inset, when compared with the single layer YBCO film 1 L, the $J_c(0)$ is increased $\approx 39\%$ and $\approx 30\%$ in films 4 L:VAC and 8 L:VAC, respectively. However, the vacuum-multilayering has a decreasing effect on B^*, since its value is highest in film 1 L. Above 1 T, all the $J_c(B)$ curves follow each other, showing that the multilayering and the sequential vacuum treatment are insignificant in terms of flux pinning.

As in magnetically measured $J_c(B)$ curves above 1 T, the similar tendency can also be seen in the angular dependent $J_c(\theta)$ curves carried out in high magnetic fields, where the absolute J_cs do not differ from each other in (Fig. 5). When looking at the shape differences of the $J_c(\theta)$ curves, we can see that the multilayering clearly improves the symmetry of the c-axis peak. The asymmetry of the $J_c(\theta)$ curve, especially in the vicinity of YBCO c-axis, can be explained by the film growth on the inclined buffer layer structure formed during the IBAD process, forming grain boundaries tilted from the normal vector of the surface [43], [44]. The formation of the c-axis peak is

earlier connected to our nanograined target material, which in addition to reduced grain boundary transfer [7] decreases the twin domain size, leading to greater number of twin boundaries and other threading dislocations along the YBCO c-axis [39], [45]. In summary, we can conclude that the self-field properties are unquestionably improved by vacuum-multilayering, which originate from the modified coherence length and penetration depth, and lengthening the electron mean free path of YBCO.

C. Mechanism of Advanced Film Growth by Vacuum Annealing

Next, we will strive to explain the underlying mechanism behind vacuum-layering deposition that ultimately results in improved crystalline quality. In order to do this, we have deposited a film corresponding to the 4 L:VAC but instead of pumping the vacuum between ablation intervals the pressure of oxygen within the deposition chamber was kept constant for the 2 min period. The magnetically measured critical current density at zero field was in this multilayer film substantially lower, showing only $\approx 7\%$ improvement when compared with the 4 L:VAC-film with almost $\approx 40\%$ improvement to the single layer film 1 L. This suggests that the modification of crystalline structure happens solely via desorption of unit structures when the vacuum treatment takes place. It is evident that under vacuum the surface of the film becomes more susceptible to the desorption of units of film structure. The desorption is more likely to happen for weakly bound species associated with dislocations in their vicinity. Thus, the vacuum-treatment could be expected to reduce the number of dislocated unit cells near the surface of film. This would naturally diminish the dislocation induced absorption of other deformed structures of the unit. Vice versa, the adsorption of well-structured units would be enhanced during the upcoming round of ablation. This model would qualitatively explain why the chains of edge dislocation were observed only for the 1L-film while for the 4 L:VAC-film they were completely absent (Fig. 3).

In order to provide further quantitative proof for the above described model, we have modelled the vacuum-multilayering deposition process by Kinetic Monte Carlo (KMC) based model [46]. The KMC simulations are based on a discrete grid
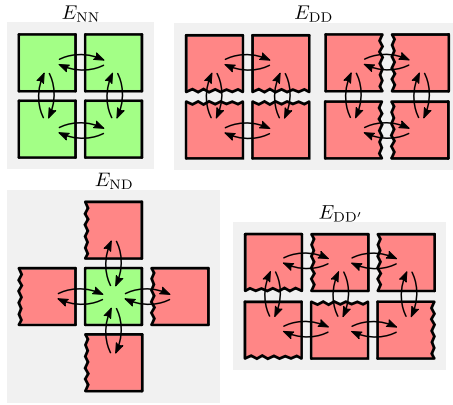
Fig. 6. A schematic illustration of the adhesion energies associated with different configurations of particles within the performed KMC simulations. The green squares indicate normal unit cells (N) while the red squares indicate dislocated unit cells (D). The dislocations can be located either left, right, top or bottom of the square and are respectively indicated by serrated lines. The adhesion energies used in the simulation fulfill the criterion $E_{NN} > E_{DD} > E_{ND} > E_{DD'}$.

Fig. 7. (a) The normalized crystalline quality as a function of film thickness for normal (NORM.) and vacuum treated (VAC-N_{vac}/N_{abl}) KMC simulations. The solid curves represent the average crystalline quality and film thickness while the error bars indicate the associated standard errors. (b) Tomographies of the simulated films resulting from normal and vacuum treated growth ($N_{vac} = 300$). The red regions illustrate the dislocations oriented along the y-direction of the grid (c-axis) while the blue regions are associated with defects along the x-direction (a/b-axis). The black solid line illustrates the surface of the film.

of arbitrary units of structure. The evolution of film growth (or corrosion) is then simulated by iterating the following algorithm: i) List all plausible adsorption (or desorption) events for the current grid, ii) determine the adhesion energies associated with the events based on the interaction of nearby units, iii) update the grid by stochastically choosing an event weighted by the previously determined energies.

Here, we have considered a total of five structures of units, including a single normal unit (N) along with four distinct dislocated units (D). The dislocated units differ from each other by the location of the dislocation that can take place either at the top, bottom, left or right side of the unit. Note that we do not address the exact physical correspondence of the associated structures of the unit due to the complexity of the PLD deposition process. Thus, the adhesion energies between these units are ultimately arbitrary. However, one can intuitively propose that the adhesion energy between two normal units (E_{NN}) is greater than between normal and any dislocated unit (E_{ND}). Moreover, the E_{NN} is evidently greater when compared with the adhesion energy between any of the dislocated unit cells. We specify these energies as E_{DD} and $E_{DD'}$ corresponding to different locations of the associated dislocations as illustrated in Fig. 6. We find it rather natural to assume that $E_{DD} > E_{ND}$ meaning that the existing units within the grid induce the adsorption of similar units in their vicinity. Correspondingly, we further assume that $E_{DD} > E_{DD'}$. These assumptions are directly linked to the experimentally observed formation of edge dislocation chains for the 1L-film (Fig. 3). In summary, the associated adhesion energies should fulfill

$$E_{NN} > E_{DD} > E_{ND} > E_{DD'}. \tag{1}$$

With the previous conclusions in mind, we have semi-arbitrarily chosen $E_{NN} = 1$, $E_{DD} = 0.7$, $E_{ND} = 0.03$ and $E_{DD'} = 0.01$. In particular, with the associated choice of energies the simulation coincides with the experimentally observed results for 1 L by the formation of the c-axis oriented chains of dislocated units.
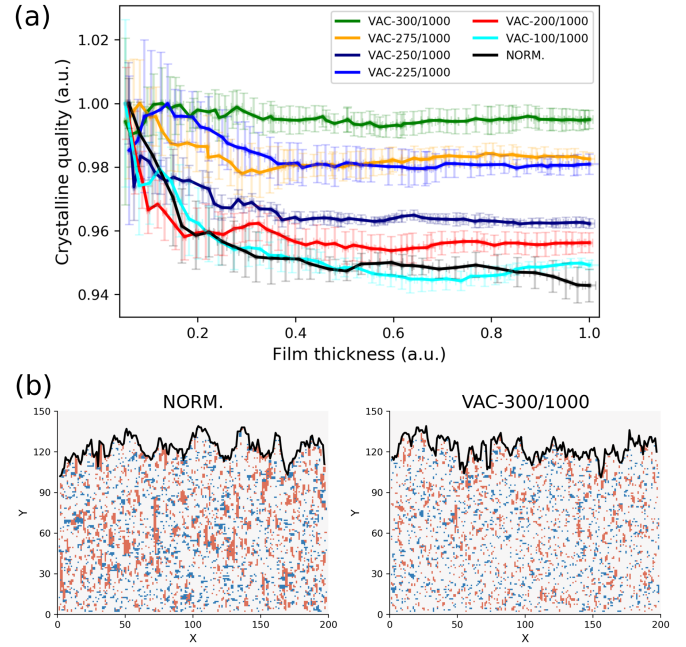
The total adhesion energy of a unit (E_{tot}) is calculated as the sum of the adhesion energies of four nearest neighbours. In the case of desorption processes, the associated event probabilities had to be weighted using energy $E_{base} - E_{tot}$, where the base energy $E_{base} = 3.1$ is arbitrary as long as it is greater than the maximum possible E_{tot}.

We have used a 200×130 sized grid that compromises between the computational efficiency and statistical relevance of the results. The grid was initialized with the 2-layers of normal units, on top of which the particles were ablated using a total of $N_{abl} = 1000$ iterations. We have allowed desorption processes during the ablation with a 20% probability. The vacuum treatment was modelled as a total of N_{vac} iterations during which the particles were solely desorbed from the surface. The ablation-vacuum treatment process was then repeated until the average thickness of the film had reached 120 units. We have probed the crystalline quality of the resulting films by calculating the relative amount of N-unit with respect to the whole film. Fig. 7(a) presents the simulated crystalline quality as a function of film thickness for both normal and vacuum-treated samples with different N_{vac} ranging between 100–300. The increase of the ratio N_{vac}/N_{abl} can be observed to lower the decay rate of crystalline quality as the film grows until it remains somewhat constant for $N_{vac} = 300$.

Fig. 7(b) further illustrates the distribution of differently oriented defects within the normal and vacuum-treated ($N_{VAC} = 300$) films. One can observe that the vacuum treatment results in

the substantial decrease of vertically (*c*-axis) oriented defects, in particular, similarly what was seen in the TEM images presented in Fig. 3. Therefore, we conclude that the vacuum layering improves the crystalline quality eminently via desorption of weakly bound atomic species, which reduces the number of dislocations near the surface of the film resulting in smaller probability of dislocation formation during the upcoming ablation interval.

IV. CONCLUSION

We have studied the effect of sequential multilayering together with vacuum treatment during the layer intervals in the growth of YBCO thin films. Based on our detailed structural analysis, we have shown that the multilayering unambiguously improves the growth mechanism by enhancing the crystalline quality and decreasing the defect formation along the YBCO *c*-axis. The improved structural properties lead to clearly increased self-field J_c. We argue, that the underlying mechanism behind the vacuum treatment is related to desorption of weakly bound atomic species from the film surface resulting in reduced probability of dislocation formation in the upcoming ablation interval. This ultimately results in the experimentally observed improved epitaxial growth of the film.

REFERENCES

[1] D. Larbalestier, A. Gurevich, D. M. Feldmann, and A. Polyanskii, "High-T_c superconducting materials for electric power applications," *Nature*, vol. 414, pp. 368–377, 2001.

[2] S. Kang et al., "High performance high-T_c superconducting wires," *Science*, vol. 311, pp. 1911–1914, 2006.

[3] C. V. Varanasi, J. Burke, L. Brunke, H. Wang, M. Sumption, and P. N. Barnes, "Enhancement and angular dependence of transport critical current density in pulsed laser deposited $YBa_2Cu_3O_{7-x}BaSnO_3$ films in applied magnetic fields," *J. Appl. Phys.*, vol. 102, 2007, Art. no. 063909.

[4] S. H. Wee, A. Goyal, Y. L. Zuev, and C. Cantoni, "High performance superconducting wire in high applied magnetic fields via nanoscale defect engineering," *Supercond. Sci. Technol.*, vol. 21, 2008, Art. no. 092001.

[5] X. Obradors and T. Puig, "Coated conductors for power applications: Materials challenges," *Supercond. Sci. Technol.*, vol. 27, 2014, Art. no. 044003.

[6] A. C. Wulff, A. B. Abrahamsen, and A. Insinga, "Topical review: Multifilamentary coated conductors for ultra-high magnetic field applications," *Supercond. Sci. Technol.*, vol. 34, 2021, Art. no. 053003.

[7] M. Z. Khan et al., "Strongly enhanced growth of high-temperature superconducting films on an advanced metallic template," *Cryst. Growth Des.*, vol. 22, pp. 2097–2104, 2022.

[8] A. Stangl, A. Palau, G. Deutscher, X. Obradors, and T. Puig, "Ultra-high critical current densities of superconducting $YBa_2Cu_3O_{7-\delta}$ thin films in the overdoped state," *Sci. Rep.*, vol. 11, 2021, Art. no. 8176.

[9] P. Paturi and H. Huhtinen, "Roles of electron mean free path and flux pinning in optimizing the critical current in YBCO superconductors," *Supercond. Sci. Technol.*, vol. 35, 2022, Art. no. 065007.

[10] E. Rivasto, T. Hynninen, H. Huhtinen, and P. Paturi, "Optimization of high-temperature superconducting bilayer structures using a vortex dynamics simulation," *J. Phys. Condens. Matter*, vol. 35, 2022, Art. no. 075701.

[11] A. Goyal et al., "Irradiation free, columnar defects comprised of self-assembled nanodots and nanorods resulting in strongly enhanced flux pinning in $YBa_2Cu_3O_{7-\delta}$ films," *Supercond. Sci. Technol.*, vol. 18, pp. 1533–1538, 2005.

[12] J. L. MacManus-Driscoll et al., "Guidelines for optimizing random and correlated pinning in rare-earth-based superconducting films," *Supercond. Sci. Technol.*, vol. 19, pp. S55–S59, 2006.

[13] S. R. Foltyn et al., "Materials science challenges for high-temperature superconducting wire," *Nature Mater.*, vol. 6, pp. 631–642, 2007.

[14] B. Maiorov et al., "Synergetic combination of different types of defect to optimize pinning landscape using $BaZrO_3$-doped $YBa_2Cu_3O_7$," *Nature Mater.*, vol. 8, pp. 398–404, 2009.

[15] M. M. Aye, M. Z. Khan, E. Rivasto, J. Tikkanen, H. Huhtinen, and P. Paturi, "Role of columnar defect size in angular dependent flux pinning properties of YBCO thin films," *IEEE Trans. Appl. Supercond.*, vol. 29, Aug. 2019, Art. no. 8000805.

[16] M. M. Aye et al., "Multilayering BZO nanocolumns with different defect densities for YBCO high field applications," *New J. Phys.*, vol. 23, 2021, Art. no. 113031.

[17] M. M. Aye et al., "Optimized $BaZrO_3$ nanorod density in $YBa_2Cu_3O_{6+x}$ matrix for high field applications," *Supercond. Sci. Technol.*, vol. 35, 2022, Art. no. 075006.

[18] G. Blatter, M. Feigel'man, V. Geshkenbein, A. Larkin, and V. Vinokur, "Vortices in high-temperature superconductors," *Rev. Modern Phys.*, vol. 66, pp. 1125–1388, 1994.

[19] T. Matsushita, *Flux Pinning in Superconductors*. Berlin, Germany: Springer, 2007.

[20] E. F. Talantsev and J. L. Tallon, "Universal self-field critical current for thin-film superconductors," *Nature Commun.*, vol. 6, 2015, Art. no. 7820.

[21] E. F. Talantsev, W. P. Crump, and J. L. Tallon, "Universal scaling of the self-field critical current in superconductors: From sub-nanometre to millimetre size," *Sci. Rep.*, vol. 7, 2017, Art. no. 10010.

[22] B. Holzapfel, B. Roas, L. Schultz, P. Bauer, and G. Saemann-Ischenko, "Off-axis laser deposition of $YBa_2Cu_3O_{7-\delta}$ thin films," *Appl. Phys. Lett.*, vol. 61, pp. 3178–3180, 1992.

[23] Z. Trajanovic, L. Senapati, R. P. Sharma, and T. Venkatesan, "Stoichiometry and thickness variation of $YBa_2Cu_3O_{7-x}$ in off-axis pulsed laser deposition," *Appl. Phys. Lett.*, vol. 66, pp. 2418–2420, 1995.

[24] B. C. Min, Y. H. Choi, S. H. Moon, S. M. Lee, S. Y. Lee, and B. Oh, "Double-sided YBCO thin films made by off-axis pulsed laser deposition," *Supercond. Sci. Technol.*, vol. 14, pp. 543–547, 2001.

[25] T. Donchev et al., "YBCO/LSMO and LSMO/YBCO double-layer deposition by off-axis magnetron sputtering and strain effects," *Vacuum*, vol. 69, pp. 243–247, 2003.

[26] E. Backen et al., "Improved pinning in YBCO based quasi-multilayers prepared by on- and off-axis pulsed laser deposition," *IEEE Trans. Appl. Supercond.*, vol. 17, no. 2, pp. 3733–3736, Jun. 2007.

[27] J. K. Chung et al., "Use of $SrTiO_3$ as a single buffer layer for RABiTS YBCO coated conductor," *IEEE Trans. Appl. Supercond.*, vol. 15, pp. 3020–3023, Jun. 2005.

[28] J. Xiong et al., "A novel process for CeO_2 single buffer layer on biaxially textured metal substrates in YBCO coated conductors," *Supercond. Sci. Technol.*, vol. 19, pp. 1068–1072, 2006.

[29] B. Maiorov et al., "Influence of naturally grown nanoparticles at the buffer layer in the flux pinning in YBCO coated conductors," *Supercond. Sci. Technol.*, vol. 19, pp. 891–895, 2006.

[30] Y. Zhao, L. Ma, W. Wu, H.-L. Suo, and J.-C. Grivel, "Study on advanced $Ce_{0.9}La_{0.1}O_2/Gd_2Zr_2O_7$ buffer layers architecture towards all chemical solution processed coated conductors," *J. Mater. Chem. A*, vol. 3, pp. 13275–13282, 2015.

[31] T. Wang, Z. Li, J. Cao, and X. Gou, "Mechanical damage of YBCO-coated conducting film caused by its CeO_2 interface with defects," *Int. J. Appl. Mech.*, vol. 11, 2019, Art. no. 1950038.

[32] Y. Takamura, N. Yamaguchi, K. Terashima, and T. Yoshida, "High-rate deposition of YBCO films by hot cluster epitaxy," *J. Appl. Phys.*, vol. 84, pp. 5084–5088, 1998.

[33] G. Koster, G. J. H. M. Rijnders, D. H. A. Blank, and H. Rogalla, "Imposed layer-by-layer growth by pulsed laser interval deposition," *Appl. Phys. Lett.*, vol. 74, pp. 3729–3731, 1999.

[34] Y. Wu et al., "Ultra-fast growth of cuprate superconducting films: Dual-phase liquid assisted epitaxy and strong flux pinning," *Mater. Today Phys.*, vol. 18, 2021, Art. no. 100400.

[35] Q. X. Jia, S. R. Foltyn, P. N. Arendt, and J. F. Smith, "High-temperature superconducting thick films with enhanced supercurrent carrying capability," *Appl. Phys. Lett.*, vol. 80, pp. 1601–1603, 2002.

[36] S. R. Foltyn et al., "Overcoming the barrier to 1000 A/cm width superconducting coatings," *Appl. Phys. Lett.*, vol. 87, 2005, Art. no. 162505.

[37] Y. L. Cheung, I. P. Jones, J. S. Abell, T. W. Button, and E. F. Maher, "Choice of insulating layer for YBCO in a multilayer architecture on buffered RABiTS," *Supercond. Sci. Technol.*, vol. 20, pp. 216–221, 2007.

[38] Y. L. Cheung, E. F. Maher, J. S. Abell, I. P. Jones, and Y. Y. Tse, "Microstructural study of a YBCO multilayer coated conductor cylinder," *Supercond. Sci. Technol.*, vol. 20, pp. 511–515, 2007.

[39] M. M. Aye et al., "Control of the nanosized defect network in superconducting thin films by target grain size," *Sci. Rep.*, vol. 11, 2021, Art. no. 6010.

[40] H. Palonen, H. Huhtinen, M. A. Shakhov, and P. Paturi, "Electron mass anisotropy of $BaZrO_3$ doped YBCO thin films in pulsed magnetic fields up to 30 T," *Supercond. Sci. Technol.*, vol. 26, 2013, Art. no. 045003.

[41] C. Cai, B. Holzapfel, J. Hänisch, L. Fernandez, and L. Schultz, "Magnetotransport and flux pinning characterictics in RBaCuO (R=Gd,Eu,Nd) and $(Gd_{1/3}Eu_{1/3}Nd_{1/3})$BaCuO high-$T_c$ superconducting thin films on $SrTiO_3$," *Phys. Rev. B*, vol. 69, 2004, Art. no. 104531.

[42] H. Huhtinen, K. Schlesier, and P. Paturi, "Growth and c-axis flux pinning of nanostructured YBCO/BZO multilayers," *Supercond. Sci. Technol.*, vol. 22, 2009, Art. no. 075019.

[43] S. H. Wee, Y. L. Zuev, C. Cantoni, and A. Goyal, "Engineering nanocolumnar defect configurations for optimized vortex pinning in high temperature superconducting nanocomposite wires," *Sci. Rep.*, vol. 3, 2013, Art. no. 2310.

[44] B. Maiorov, B. Gibbons, S. Kreiskott, V. Matias, T. Holesinger, and L. Civale, "Effect of the misalignment between the applied and internal magnetic fields on the critical currents of tilted coated conductors," *Appl. Phys. Lett.*, vol. 86, 2005, Art. no. 132504.

[45] M. Z. Khan et al., "Enhanced flux pinning isotropy by tuned nanosized defect network in superconducting $YBa_2Cu_3O_{6+x}$ films," *Sci. Rep.*, vol. 9, 2019, Art. no. 15425.

[46] D. Landau and K. Binder, *A Guide to Monte Carlo Simulations in Statistical Physics*. Cambridge, MA, USA: Cambridge Univ. Press, 2021.